Particle Accelerators
1980, Vol. 11, pp. 113-123
0031-2460/80/1102-0113 $06.50/0

AN ESTIMATE OF THE POTENTIALS OF A MAGNETIC LINEAR ACCELERATOR (MAGLAC)

F. ARENDT

Kernforschungszentrum Karlsruhe GmbH, Institut f. Technische Physik 7500 Karlsruhe, Postfach 3640, Federal Republic of Germany

(Received March 4, 1980)

The possibilities of utilizing a Magnetic Linear Accelerator (MAGLAC) for macroparticles to compress and heat fusion fuel pellets are discussed. The performance of a MAGLAC driver is limited by the properties of conceptual projectiles and by magneto-mechanical stresses occurring in the accelerator coils. Superconducting projectiles are shown to remain stable and intact at acceleration rates below 10^6 m/s^2, while ferromagnetic projectiles may experience acceleration rates up to 2×10^6 m/s^2. Their design will be quite complicated, with laminated, high-resistivity materials required. A number of issues in accelerator technology are listed that must be solved prior to establishing a MAGLAC for acceleration rates required for "Impact Fusion".

1. INTRODUCTION

In recent publications and discussions[1-3] a new scheme for achieving controlled thermonuclear burn has been proposed; it is called "Impact Fusion". Its idea is to provide energy for compression and heating of a fuel pellet by means of the kinetic energy of a fast-moving macroparticle instead of using lasers or charged-particle beams as discussed in the concepts of inertial-confinement fusion. The supporters of impact fusion claim that energy delivery into the pellet will be straightforward without having to consider esoteric processes of magneto-hydrodynamics, as in the inertially confined schemes.

For the acceleration of the macroparticles, a traveling wave of magnetic-field gradient is proposed by which a permanent magnetic dipole can be accelerated. The propagation of the wave is controlled by the velocity and position of the dipolar projectile in such a way that a stabilized path with optimum accelerating conditions persists throughout the acceleration process.

In this note, various rough estimates given in the papers referenced above on the layout of accelerator and projectile are looked at in more detail. It turns out that from some fundamental geometric and magnetomechanical considerations, upper limits for the rate of acceleration obtainable result that could cast some doubt on the economical realizability of such a Magnetic Linear Accelerator as driver for impact fusion.

2. BASIC ASSUMPTIONS

In order to obtain some ideas of the orders of magnitudes and scales involved in a driver for impact fusion, it is useful to define some basic requirements. Lacking extensive studies on the coupling mechanisms and energy-transfer efficiency between projectiles and fusion-pellet, it seems fair to consider requirements similar to those posed in ICF proposals: kinetic energy of the projectile $T_p = 10^6$J and time of energy delivery to pellet $\tau = 10^{-8}$s.

Although it is claimed that in impact fusion the efficiency of energy delivery to the pellet is better than in ICF, the pellets will have to be of high mass to permit high gains and low repetition rates in a reactor. Low repetition rates are desirable from an economic point of view to keep small the relative cost contribution from those masses that have to be attached to the pellet to guarantee absorption of the projectile energy in the pellet instead of an elastic transfer of momentum. These masses will be vaporized during the fusion microexplosion and may be used again only after costly reprocessing, if at all.

From

$$T_p = 1/2\, m v_f^2 = 1/2\, \delta\, A l v_f^2 \qquad (2.1)$$

and

$$\tau = l/v_f \qquad (2.2)$$

the basic requirements are connected with the geometric and material properties of the projectile and with its final velocity. One then gets

$$l^3 = 2T_p\tau^2/\delta A. \tag{2.3}$$

Taking $\delta = 8 \times 10^3$ kg/m^3, the only variable in Eq. (2.3) is the projectile cross section A, for which a reasonable domain $10^{-6}\text{m}^2 \leq A \leq 10^{-4}$ m^2 can be assumed:

$$3 \times 10^{-3}\text{m} \geq l \geq 0.6 \times 10^{-3}\text{m}, \qquad 3 \times 10^5\text{m/s} \geq v_f \geq 0.6 \times 10^5\text{m/s}. \tag{2.4}$$

For further estimates, a typical final velocity of $v_f = 10^5$ m/s will be taken, associated with a projectile length of 1 mm and a diameter of $2r_2 \approx 6$ mm. It should be born in mind, however, that a decrease of the projectile cross-section area or of the projectile diameter leads to an increase in the required final velocity.

3. ACCELERATOR STRUCTURE

3.1 *Geometric Arrangement*

The basic philosophy of the possible structure for a magnetic linear accelerator and its operating principle is thoroughly discussed in Ref. 2 and will only be summarized here. The main idea is that a premagnetized magnetic dipole is accelerated in a magnetic gradient field. The dipole orientation is stable if the force is exerted as a drag from a magnetic pole of opposing polarity; it is unstable if it is a pushing force between two poles of the same polarity. In other words, a stably oriented dipole is pulled into a peak-field zone and not pushed away from it.

This principle is realized by a linear array of coaxial coils of, preferably, identical bore. The axis of the array coincides with the path of the projectile (Fig. 1).

3.2 *Triggering*

Each coil can be powered independently, e.g., from a charged capacitor associated with it. The L-C-circuit thus formed causes a sinusoidal time-dependence of coil current and hence of the magnetic field in the coil. In the accelerator proposed, the current in each coil flows for just one half period of the L-C-oscillation, terminating at exactly that instant of time at which the projectile passes through it. At this time, the switch between coil and capacitor is opened, leaving the electromagnetic energy of the circuit dumped back into the capacitor. Simultaneously, a switch is closed to power that coil which is a distance

$$2g = v \cdot \frac{T}{2} = v \cdot \pi \cdot \sqrt{LC} \tag{3.1}$$

ahead of the projectile position. All coils between were powered before and are in the process of executing their half-period oscillations while the other coils are idle.

This scheme ensures that the peak-field region moves a distance g ahead of the projectile with the same speed, exerting an almost constant drag. The proper relationships of projectile position and speed to powering of the various coils can be established in real time by measuring the projectile data and firing the switches accordingly. This is possible because even the peak projectile velocity of approximately 10^5 m/s is small compared with electrical signal velocities.

3.3 *Adjustment*

Essentially two ways can be conceived to adjust the accelerator circuits to the varying projectile speed along the axis as expressed by Eq. (3.1). The first one is to permit an increase in g, the gap between the peak-field region and the projectile position, as the velocity rises. This scheme is undesirable because the drag exerted on the projectile becomes smaller as g increases [see Eq. (3.5)].

The second alternative requires adjustment of C in order to keep the gap and the rate of acceleration constant. Since the energy $1/2\ CU^2$ stored in a capacitor remains constant along the accelerator if the coils are identical and since the same peak field is desired everywhere, the voltage U at the capacitors varies proportional to velocity to have $v \cdot C^{1/2} = \text{const}$. This alternative means that during the entire acceleration process, the projectile travels at constant distance behind the peak-field region and is accelerated at an essentially constant rate. The real-time control of the coil powering process eliminates the danger that fluctuations in the projectile injection velocities could cause a stop to the acceleration due to a quadratic increase in the gap between the positions of projectile and peak field region, as might be encountered with a pre-programmed firing of the L-C circuits. With these advantages and no

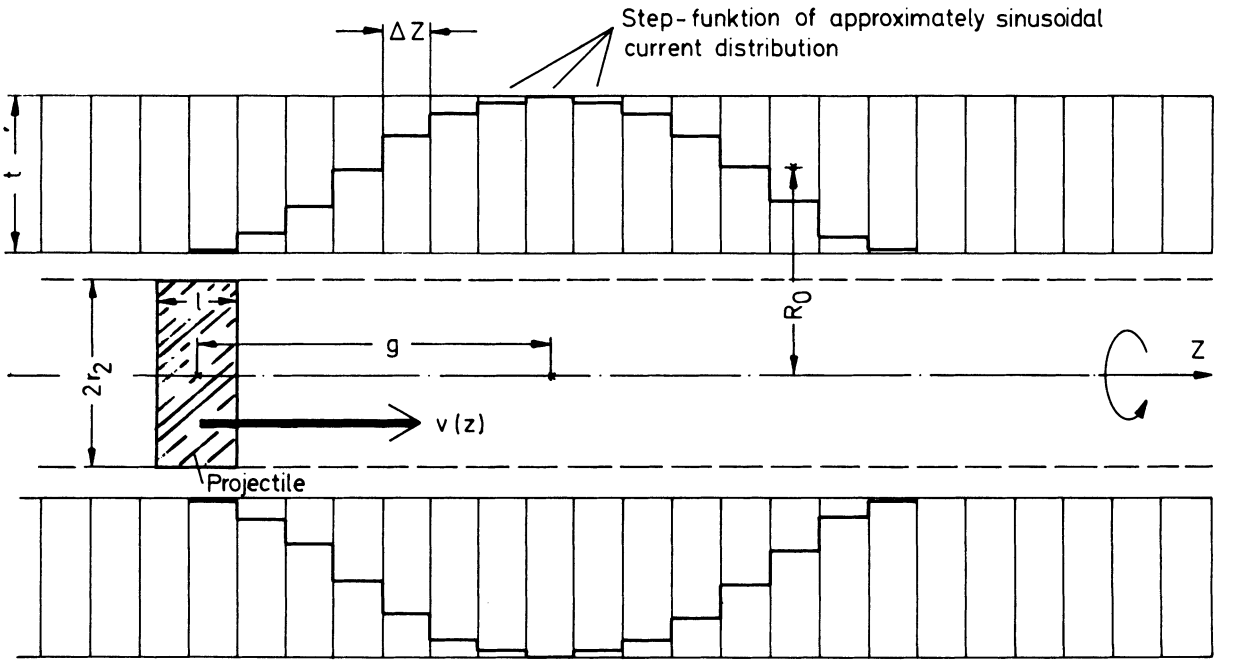

FIGURE 1 Geometric arrangement of a conceptual Magnetic Linear Accelerator.

obvious drawbacks, except the fine adjustment of capacitors, the second alternative will be favored in this discussion.

Eq. (3.1) permits as a theoretical third choice the variation of the coil inductance. This can essentially be achieved only by altering the coil diameter which would lead to decreased accelerating rates, larger stored energies in capacitors resp. coils even with peak-field level maintained, and larger Joule losses as compared to an accelerator of minimum coil diameter.

In conclusion, it can be stated that the capacitor for every single coil must be adjusted in such a way that the current flows according to

$$I = I_0 \cdot \sin\left(\pi \cdot \frac{v(z)}{2g} \cdot t\right); 0 \leq t \leq \frac{2g}{v(z)}. \quad (3.2)$$

The current amplitude I_0 determines the peak magnetic field in the coil.

3.4 *Magnetic Field and Gradient*

The exact space and time dependence of field and field gradient at the location of the projectile must be calculated in detail for each accelerator structure foreseen. However, a number of rough estimates are possible that describe reality within a factor of 2 and are thus sufficient for assessing the virtues of the MAGLAC principle.

At any given moment, the current variation of Eq. (3.2) in a number of adjacent coils will cause a corresponding spatial variation of current, approximately as a sinusoidal half wave parallel to the axis. The peak field is attained in the center of this wave, i.e., in the coil at distance g downstream from the projectile. The level of peak field depends on two parameters, the total number of coils activated at a given moment, and the ratio between g and the mean radius R_0 of the coils. Peak acceleration rates are attained at $R_0/2 \leq g \leq R_0$ [see Eq. (3.5)].

For technical reasons, only a small finite number of coils can be established between projectile and peak-field region since each coil requires an independent switch and capacitor. Ideally, a smooth approximation of a sinusoidal half-wave by an infinite number of coils would be required; in that case, the projectile in flight would not experience any *ac* component in the magnetic field. *AC* components give rise to eddy currents and hysteric losses in the projectile and should therefore be kept as low as possible. As many coils as technically possible are therefore desired with a minimum of 5 within a distance of $2g$.

Several magnetic-field calculations have been performed within the parameter range $R_0/2 \leq g \leq R_0$ and $5 \leq N \leq 10$ coils within a distance of $2g$. They indicate that within the factor of 2 mentioned above, the peak field is given by

$$B_0 = 1/2\ \mu_0 j_0 t, \tag{3.3}$$

which corresponds to one-half the field level attained in an infinitely long solenoid of peak current density j_0 and thickness t. Simultaneously, the field along the axis is well approximated by the field of a circular current loop

$$B(z) = B_0 \cdot \left[\frac{R_0}{(R_0^2+z^2)^{1/2}}\right]^3, \tag{3.4}$$

where z is taken along the axis with $z = 0$ at peak-field position. The field gradient, which is a key parameter (proprotional to the force or to the rate of acceleration) then reads

$$\frac{dB(z)}{dz} = B_0 \cdot \left[\frac{R_0}{(R_0^2+z^2)^{1/2}}\right]^3 \cdot \frac{-3z}{R_0^2+z^2} = \frac{-3z}{R_0^2+z^2} \cdot B(z) \tag{3.5}$$

This function attains a maximum at $z = \pm R_0/2$. As shown in Ref. 2, the projectile must travel behind this maximum to ensure transverse stability of its motion while the longitudinal stability is guaranteed by the real-time control scheme discussed in Section 3.2. The optimum position for the center of a ferromagnetic projectile is thus at $g = -R_0/2$, giving a local field gradient of

$$\frac{dB(-R_0/2)}{dz} = \frac{2^3 \cdot 3 \cdot 2}{5^{3/2} \cdot 5} \cdot \frac{B_0}{R_0} \approx 0.86 \cdot \frac{B_0}{R_0}. \tag{3.6}$$

For a superconducting projectile, the current density and thus the magnetic dipole moment attainable are related to the field at the projectile by the $j_c - B$ curve for hard superconductors ("pinning force"). It is worthwhile to note that the maximum of $[dB(z)/dz]/B(z)$ is situated at $z = \pm R_0$: at this point a maximum rate of acceleration is provided for least field. For a superconducting projectile, one would therefore select $g = -R_0$, twice the gap of a ferromagnetic dipole, with

$$\frac{dB(-R_0)}{dz} = \frac{3}{4\sqrt{2}} \cdot \frac{B_0}{R_0} \approx 0.53 \cdot \frac{B_0}{R_0} = 1.50 \cdot \frac{B(-R_0)}{R_0} \tag{3.7}$$

This choice has the additional advantage that more coils can be provided between projectile and peak-field region, smoothing out the *ac* components of field, to which a superconducting projectile is particularly sensitive.

4. PROJECTILES AND ACCELERATION RATES

Various ideas have been proposed for optimizing the projectile design with respect to efficiencies of energy transfer to conceptual pellets. These geometric details essentially do not influence the projectile parameters relevant for the accelerating phase. The rough dimensions were estimated in Section 2; this paragraph reviews the additional constraints imposed on the accelerating rate by the magnetic properties of the projectile.

In the linear coil array considered, the axial force on a magnetic dipole with dipole moment μ is given by

$$F_z = \mu \cdot \frac{dB_z}{dz}. \tag{4.1}$$

The dipole moment is expressed by

$$\mu = \frac{1}{\mu_0} \cdot \phi l = \frac{B_p}{\mu_0} \cdot Al = \frac{B_p}{\mu_0} \cdot V, \tag{4.2}$$

where B_p is the magnetic induction permanently "frozen" into the projectile at the start of acceleration, and l,A,V are the length, cross-section area, and volume of the projectile. Two alternatives for the projectile material were proposed, ferromagnetic material with a saturation induction B_{sat}, and a superconducting miniature solenoid in which the dipole flux is produced by a current flowing about the coil axis which coincides with the accelerator axis. For the sake of this discussion, it is assumed that the entire projectile volumes are magnetically active.

4.1 *Ferromagnetic Projectile*

The peak magnetic induction is given by B_{sat}. Using Eqs. (3.6), (4.1), (4.2), and $a = F_z/\delta \cdot V$ to give the acceleration rate, one has

$$a = \frac{1}{\mu_0} \cdot \frac{B_{sat}}{\delta} \cdot 0.86 \frac{B_0}{R_0} \approx 7 \times 10^5 \cdot \frac{B_{sat} \cdot B_0}{\delta \cdot R_0} \quad (4.3)$$

In discussing the disadvantages of ferromagnetic projectiles, two aspects are usually mentioned, the low saturation induction, a maximum of the order of 3 T, and the danger of evaporating the projectile in flight by eddy-current heating induced by the *ac* component caused by the finite number of activated coils.

While the significance of a limited B_{sat} can be assessed only in comparing it to the acceleration rates achievable with superconducting projectiles, *ac* heating may in principle be reduced by three measures, maximum possible number of activated coils, laminated projectile, and use of low electrical-conductivity material for projectiles, such as ferrites. All three measures can be applied, but significantly influence the economics of an impact fusion scheme. As the local rate of acceleration varies along the length of a projectile due to the z-dependence of the field gradient of Eq. (3.5), particular care must be taken in selecting bonding techniques for laminated parts and material properties of ferrites. Neglect of these aspects may cause the projectile to disintegrate physically in flight.

4.2 *Superconducting Projectile*

A superconducting projectile is usually envisaged as a solenoid at cryogenic temperature in which an azimuthal current of current density j generates the magnetic dipole moment (Fig. 2). A first quantitative estimate assumes that the projectile is infinitely long, yielding

$$\begin{aligned} B_z(r) &= \mu_0 j(r_2 - r_1), \; r \le r_1 \\ B_z(r) &= \mu_0 j(r_2 - r), \; r_1 \le r \le r_2. \end{aligned} \quad (4.4)$$

From this, the total flux for infinite projectile length is

$$\phi(\infty) = \int_0^{r_2} 2\pi r \cdot B(r) \cdot dr = \frac{\pi}{3} \mu_0 j \cdot (r_2^3 - r_1^3),$$

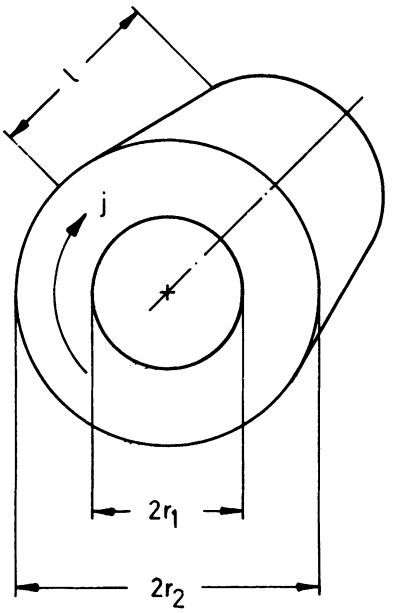

FIGURE 2 Sketch of superconducting projectile.

which has a maximum at $r_1 = 0$. Using this maximum value implies that the total cross section of the projectile carries current. However, a more realistic design basis of $r_1 \approx r_2/2$ reduces the total flux by only about 10%. Within the scope of this note, it is therefore justified to use the maximum flux. The actual flux must be reduced by effects of finite projectile length. Taking $l = 2r_2$ which gives a larger flux than the more realistic $l = 1/3r_2$ derived in Section 2, the maximum flux must be reduced to 2/3.

$$\phi = \frac{2}{3} \cdot \frac{\pi}{3} \mu_0 j r_2^3 \approx \frac{\pi}{5} \mu_0 j r_2^3. \quad (4.5)$$

Combining Eqs. (4.2) and (4.5) gives a dipole moment

$$\mu = \pi r_2^2 \cdot l \, j \cdot \frac{r_2}{5} = \pi r_2^2 l \cdot \frac{F_v}{B_{sc}} \cdot \frac{r_2}{5},$$

which together with Eqs. (3.7) and (4.1), determines the rate of acceleration for superconducting projectiles

$$a = \frac{1.5}{5\delta} F_v \cdot \frac{r_2}{R_0} \cdot \frac{B(-R_0)}{B_{sc}} = \frac{0.3}{\delta} F_v \frac{r_2}{R_0} \cdot \frac{B(-R_0)}{B_{sc}}. \quad (4.6)$$

The meaning of the newly introduced terms F_v and B_{sc} is discussed below.

The volume pinning force F_v is a microstructure-dependent property of the superconducting material of the projectile. It is obtained experimentally from the critical current density at a given field level

$$F_v = j_c(B) \cdot B. \tag{4.7}$$

This definition characterizes F_v as a Lorentz force density exerted on the magnetic flux lines pinned by the superconductor. It increases with the density of pinning centers (such as precipitates and grain boundaries) and the average elementary pinning strength of each center. The gross shape of the function $F_v(B)$ can be made plausible by considering the finite critical current density at zero field [$j_c(O) < \infty$] and the existence of an upper critical field B_{c2} at which $j_c(B_{c2}) = 0$. With $F_v(O) = F_v(B_{c2}) = 0$, the function must have a maximum between. For typical superconductors investigated today, the maximum is located near $b_p \equiv B_{max}/B_{c2} = 0.2 \ldots . 0.4$. For B approaching B_{c2}, the dependence of F_v on B is expressed by [4]

$$F_v(b) = \frac{F_{vmax}}{0.286} \cdot b^{1/2}(1-b)^2, \; b \to 1, \tag{4.8}$$

with $b = B/B_{c2}$, the field normalized to critical field (Fig. 3). It is assumed in the further discussion that for superconductors with very high pinning, as considered in this note, Eq. (4.8) describes the relationship between F_v and b for $b \geq b_p = 0.2$.

Today, typical advanced superconductors such as Nb_3Sn and other $A15$-compounds have maximum volume pinning forces of several $10^{10} N/m^3$ at 4.2 K. It is therefore a very optimistic assumption to use $F_{vmax} = 10^{11}$ N/m^3 as an upper limit even at 2 K, regarding the fact that stabilizing and structural materials incorporated into the superconducting compound reduce the overall critical current density considerably. This limit is also justified from a mechanical point of view, because the peak hoop stress in the projectile is of the order of

$$\sigma_{max} \approx F_v \cdot r_2.$$

With r_2 of the order of several millimeters, as discussed in Section 2, stresses of some 10^8 N/m^2 are encountered in the projectile. It is clear that

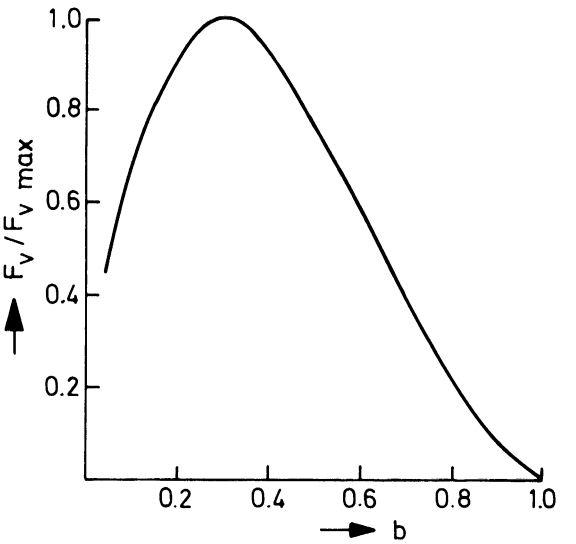

FIGURE 3 Gross shape of volume pinning force vs reduced critical field.

stresses of such magnitude will cause severe mechanical problems, especially when recalling that hard superconductors must have a highly inhomogeneous structure to provide for pinning centers. Mechanically reinforcing and electrically stabilizing materials and refrigerants which, conceptually, must be added to the pure superconductor to overcome these problems and keep it superconducting during the acceleration phase, will deteriorate the average volume pinning force of the projectile, as mentioned before. Thus, it is in no way conservative to use a value of $\sim 10^{11}$ N/m^3 for F_{vmax}.

The second new quantity used in Eq. (4.6), B_{sc}, is the field level at the position of the superconducting projectile. It is calculated as the sum of the projectile self-field, B_{self}, and the field $B(-R_0)$ of the accelerator coils at the projectile. It is this latter contribution from the accelerator field in the denominator of Eq. (4.6) that justifies positioning the projectile at $g = R_0$ behind the peak-field region [as stated in Eq. (3.7)], rather than at the point of largest field gradient. The self-field is given by Eq. (4.4). Using $r_1 \approx r_2/2$ and replacing j by F_v/B_{sc} gives

$$B_{self} = \mu_0 \cdot \frac{F_v}{B_{sc}} \cdot \frac{r_2}{2}. \tag{4.9}$$

In summary, the rate of acceleration of Eq. (4.6)

can be optimized by using the maximum of

$$g(b) \equiv F_v \cdot \frac{B(-R_0)}{B_{sc}} = F_v \left(1 - \frac{B_{self}}{B_{sc}}\right) = F_v \left(1 - \frac{\mu_0 r_2}{2B_{c2}^2} \cdot \frac{F_v}{b^2}\right) \quad (4.10)$$

with respect to the operating field $B_{sc} = B(-R_0) + B_{self}$ or its normalized value $b = B_{sc}/B_{c2}$. With Eq. (4.8), one has

$$g(b) = \frac{F_{v\max}}{0.286}(1-b)^2 \left(b^{1/2} - \alpha \cdot \frac{(1-b)^2}{b}\right) \equiv \gamma \cdot F_{\max}, \quad (4.10')$$

with $\alpha = \dfrac{\mu_0 r_2 \cdot F_{v\max}}{0.286 \times 2B_{c2}^2}$ as parameter. With $F_{v\max} \leq 10^{11}$ N/m^3, $r_2 = 3$ mm, and $B_{c2} \geq 25$ T for advanced superconductors, one has $0 \leq \alpha \leq 1$. Table 1 gives b-values at which (4.10′) has a maximum, and the corresponding γ-factor.

For another optimistic estimate, assume $B_{c2} = 60$ T, giving $\alpha = 0.3$ and hence

$$F_v \cdot \frac{B(-R_0)}{B_{sc}} \text{ (optimum)} = \frac{1}{2} F_{v\max}. \quad (4.10'')$$

Finally, the ratio of radii r_2/R_0 in Eq. (4.6), which by nature is less than 1, is realistically estimated to 1/2. The main reason is that the projectile will not have reserves in space and mass to transport a refrigerant without diluting its average $F_{v\max}$. The projectile should therefore travel in a cold bore with its excellent vacuum properties. The bore must be shielded from the warm accelerator coils by a cryostat of a minimum thickness of a few millimeters, the same order of magnitude as the projectile radius, hence $R_0 \approx 2r_2$. It should be mentioned that the radius ratio further decreases for a realistic design of the accelerator coils, which must be made radially thick (see Section 5).

Numerical evaluation of Eq. (4.6) now yields

$$a = \frac{0{,}3}{\delta} \cdot F_v \frac{B(-R_0)}{B_{sc}} \cdot \frac{r_2}{R_0} = \frac{0{,}3}{8 \times 10^3} \cdot \frac{1}{2} \cdot 10^{11} \cdot \frac{1}{2} = 1 \times 10^6 m/s^2. \quad (4.6')$$

TABLE 1

Optimum Operating Fields $b_{\max} = B_{sc}/B_{c2}$ for Superconducting Projectiles

α	$b_{\max}$	γ
0.0	0.2	1
0.1	0.359	0.70
0.2	0.421	0.57
0.3	0.463	0.50
0.4	0.493	0.44
0.5	0.518	0.40
0.6	0.538	0.37
0.7	0.556	0.34
0.8	0.571	0.32
0.9	0.584	0.30
1.0	0.596	0.28

This value, obtained even with extremely optimistic assumptions on superconductor properties ($F_{v,\max} = 10^{11}$ N/m^3, $B_{c2} = 60$ T) is inferior to the ferromagnetic projectile acceleration of Eq. (4.3) for $B_0 \geq 12$ T. One reason is that no cryostat is required for ferromagnetic projectiles. An estimate of B_0 for the superconducting projectile conditions used in (4.6′) leads to values above 50 T. The superconducting projectile is therefore ruled out as a reasonable choice, not only because of the tremendous technological difficulties associated with its use but also because of very fundamental physical properties of superconductors.

5. ACCELERATOR COILS

With the ferromagnetic projectile remaining as the better choice, the rate of acceleration is given by Eq. (4.3) and thus determined by the accelerator parameters B_0 and R_0. B_0 is given by Eq. (3.3) as the peak field in an accelerator coil, and R_0 is the average radius of the current-carrying part of the coil. For high acceleration rates, R_0 should be as small as possible. This demand would automatically be met by using the skin effect during the very short excitation time of the coil; it confines the current to a narrow radial region around the bore. In Sections 5.1 and 5.2, the consequences of skin effect on the Joule losses and the mechanical loading of the coils are discussed. Section 5.3 outlines the design of coils that avoid skin effect and the resultant maximum acceleration rates. In all considerations, the inductive coupling between active accelerator coils is neglected, as is the loading imposed on the coil

current by the projectile. The coil bore matches the projectile diameter $2r_2 = 6$ mm.

5.1 *Joule Losses*

In each accelerator coil (Fig. 1) of axial length Δz and physical thickness t, the current is actually confined to a skin depth

$$d = \frac{1}{2\pi}\sqrt{\frac{\rho}{\nu\cdot\mu_0}} = \frac{1}{\pi}\sqrt{\frac{\rho\cdot g}{v(z)\cdot\mu_0}}, \qquad (5.1)$$

with ρ the coil-material resistivity and, according to Eq. (3.2), $\nu = v(z)/4g$ the z-dependent frequency of current rise and decay. Assuming constant current density in the skin layer d during the current pulse, the instantaneous Joule loss power is given by

$$P(z,t) = R\cdot I^2 = \rho\cdot\frac{2\pi r_2}{d\cdot\Delta z} j_0^2 d^2\cdot(\Delta z)^2\cdot \sin^2\left(\pi\cdot\frac{v(z)}{2g}t\right)$$

and the total Joule energy in a coil at position z by

$$\Delta E(z) = \int_0^{2g/v(z)} P(z,t)dt = \rho\cdot 2\pi r_2\cdot\Delta z\cdot d\cdot j_0^2\cdot\frac{g}{v(z)} \qquad (5.2)$$

$$= \frac{8\pi^2}{\mu_0} B_0^2 r_2 \sqrt{\frac{\rho g}{\mu_0}}\cdot\frac{\Delta z}{\sqrt{v(z)}},$$

where Eqs. (3.3) and (5.1) are used in the last step. The total dissipative loss is given by summing over all coils or by integrating

$$E_{\text{tot}} = \int_0^L dE(z) = \frac{8\pi^2}{\mu_0} B_0^2\cdot r_2\sqrt{\frac{g\rho}{\mu_0}}\int_0^L\frac{dz}{\sqrt{v(z)}}. \qquad (5.3)$$

This integral may be solved by assuming a constant rate of acceleration a and substituting $dz = v(z)\cdot dt = v(z)\cdot dv/a$ to give

$$\int_0^L\frac{dz}{\sqrt{v(z)}} = \frac{1}{a}\int_{v_0}^{v_f}\sqrt{v(z)}\,dv = \frac{2}{3a}(v_f^{3/2} - v_0^{3/2}) \approx \frac{2v_f^{3/2}}{3a}$$

and

$$E_{\text{tot}} = \frac{16\pi^2}{3\mu_0}\cdot\frac{B_0^2 r_2}{a}\cdot\sqrt{\frac{g\rho}{\mu_0}}\cdot v_f^{3/2} = 3.8\times 10^4\cdot\frac{B_0}{B_{\text{sat}}}\cdot r_2^{5/2}\cdot\rho^{1/2}\cdot v_f^{3/2}\cdot\delta \qquad (5.3')$$

by inserting $g = R_0/2 = r_2/2$ and Eq. (4.3). Numerical evaluation of this formula with $\rho = 2\times 10^{-8}$ Ωm and the reference data of Section 2 shows that at $B_0 = 1{,}5\times B_{\text{sat}}$ Joule losses match the kinetic energy of the projectile of 1 MJ. However, the rate of acceleration is only 4×10^5 m/s^2 for $B_{\text{sat}} = 3$ T; much too low for MAGLAC to be an economic fusion driver. Higher acceleration rates are associated with higher losses.

It is worthwhile to estimate coil heating by Joule losses from Eq. (5.2). With $\Delta E(z) = c_p\delta\cdot 2\pi r_2\cdot d\cdot\Delta z\cdot\Delta\theta$, one finds

$$\Delta\theta = \frac{4\pi^2}{c_p\delta\cdot\mu_0}\cdot B_0^2 \qquad (5.4)$$

if the skin layer is heated adiabatically. The adiabacity criterion may be released by noting that at the high-velocity end, where heating is most critical, the heat can diffuse into 30 skin depths during the coil activation time if it flows at the speed of sound. Temperature differences obtained with Eq. (5.4) may therefore be reduced by 1/30. Using $c_p\delta \approx 3\times 10^6$ Jm^{-3}K^{-1}, the correct order of magnitude for high-conductivity metals, gives $\Delta\theta = 1/30\cdot 10\,B_0^2 \approx 200$ K for B_0 of 25 T and an acceleration rate of about 2×10^6 m/s^2.

5.2 *Magnetomechanical Stresses*

Activation of the accelerator coils will create a magnetomechanical pressure shock which very roughly can be approximated by a hydrostatic pressure of magnitude $p = B_0^2/2\,\mu_0$ in the coil bore. Reason for the shock is the Lorentz-force acting on the winding from the interaction between the current and the magnetic field. Just like the Joule heat discussed in Section 5.1, the force will be carried at the speed of sound away from the skin layer, i.e., its area of origination, radially outward into the bulk material of the coil. Using the thickness of 30 skin layers as estimated above, the inside coil layer will be stressed during the current pulse to

$$\sigma = \frac{B_0^2}{2\mu_0}\cdot\frac{r_2}{t} = \frac{B_0^2}{2\mu_0}\cdot\frac{r_2}{30d}. \qquad (5.5)$$

For $B_0 = 10$ T, that is, an acceleration rate of less than 10^6 m/s^2, the initial shock stress (5.5) amounts to 8×10^8 N/m^2.

To summarize the discussion in Section 5.1 and 5.2, the utilization of skin layer current for attaining peak acceleration rates according to Eq. (4.3) is limited to unattractive parameters due to gross dissipative losses, to heating of the individual coils, and most importantly, to high shock stressing of the inside coil layer. Even when realizing that the coil will not blow apart at each cycle because the shock load will eventually be distributed in the bulk coil material, repeated shock loading with simultaneous heating will lead to cracks and fracture limiting of the coil life-time to very unattractive periods. Even though this fatigue problem is most severe only at the high-velocity end of a conceptual MAGLAC, the economics of the device as a fusion driver rule out utilization of the skin-layer current.

5.3 *Coil Concept*

The distribution of current to regions radially outside the skin layer may be achieved in two ways:

(1) Utilization of filamented conductor with filament diameters of approximately one skin depth. The filaments must be fully transposed through the conductor cross section with a transposition pitch smaller than the circumference of a coil winding in which the conductor is used. Transposition means that each filament touches both the inside and outside surfaces of the winding; it guarantees almost identical inductances for each filament and hence effective distribution of the current.

(2) Manufacture of the coils from several windings of filamented conductor. The severe disadvantage of this approach is the quadratic increase of coil inductance, which requires a quadratic decrease of capacitance and a linear increase of voltage in the storage capacitor. Even with only 5 windings, the capacitance drops to several 10^{-10}F at the high-velocity end of the accelerator with several 10^5V of voltage required. This capacitance then becomes comparable to the self-capacitance of the coil, making the triggering scheme of Section 3.2 impossible. It should be mentioned that coil self-capacitance increases with the number of windings.

In estimating the upper limit for the radial thickness of the coil, it must be realized that the maximum thickness of the filamented conductor is limited to an optimistic 20% of the winding radius to provide for transposition and to avoid filament rupture due to bending strains. With a peak number of 5 turns permitted by the voltage and capacitance argument, the coil thickness matches the bore radius, $t \approx r_2$, which together with Eq. (5.5) gives a stress in the accelerator coil

$$\sigma \approx \frac{B_0^2}{2\mu_0}$$

For engineering reasons $\sigma \leq 4 \times 10^8$ N/m^2 is required, giving $B_0 \leq 32$ T. Inserted into Eq. (4.3) with $B_{sat} = 3$ T and $R_0 = 3/2\ r_2$ for the case of a thick coil gives

$$a = 2 \times 10^6 \text{ m/s}^2$$

as the maximum rate of acceleration conceivable in a MAGLAC for impact fusion.

It should be noted that even the theoretically possible further increase in coil thickness and thus B_0 at a given peak stress does not lead to higher acceleration rates in Eq. (4.3) because $R_0 = r_2 + t/2$ increases in parallel. Dissipative losses and Joule heating of individual coils are insignificant in a thick-coil accelerator, as long as the resistivity is below 5×10^{-8} Ωm.

6. TENTATIVE PARAMETERS

The arguments put forward in this note are best summarized in Table 2 by a list of tentative, though very optimistic parameters for a conceptual MAGLAC for impact fusion.

7. CONCLUDING REMARKS

The discussion of the MAGLAC principle shows that its utilization as a driver for impact fusion meets severe economic and technological problems. The complexity of the device is at least comparable to that of other conceptual fusion drivers. As superconducting projectiles are clearly inferior to ferromagnetic ones, which are much more simple to produce, any research work that may be foreseen in this area should concentrate on the technology of the accelerator itself. Here

TABLE 2
Parameters for a Tentative Fusion Driver

Basic requirements and projectile			
Kinetic energy of projectile	T_p	10^6	J
Energy delivery time	τ	10^{-8}	s
Density of projectile	δ	8×10^3	kg m^{-3}
Radius of projectile	r_2	3×10^{-3}	m
Length of projectile	l	1×10^{-3}	m
Final velocity	v_f	10^5	ms^{-1}
Material of projectile		ferromagnetic, high resistivity, possibly laminated	
Saturation induction	B_{sat}	3	T
Accelerator coils			
Shape		solenoidal	
Bore radius	r_2	3×10^{-3}	m
Radial thickness	t	3×10^{-3}	m
Effective mean radius	R_0	4.5×10^{-3}	m
Peak magnetic induction	B_0	32	T
Peak current density	j_0	1.7×10^{10}	Am^{-2}
Peak current	I_0	3×10^4	A
Axial width	Δz	$<6 \times 10^{-4}$	m
Excitation time	$T/2$	$>3 \times 10^{-8}$	s
Peak hoop stress	σ	4×10^8	Nm^{-2}
Coil inductance for 5 windings	L	2.7×10^{-7}	Hy
Stored energy per coil	W	120	J
Capacitance of storage	C	$>4 \times 10^{-10}$	F
Voltage of storage	U	$<8 \times 10^5$	V
Rate of acceleration	a	2×10^6	ms^{-2}
Length of accelerator	L	2.5×10^3	m
Number of coils, capacitors, and switches	$L/\Delta z$	$>4 \times 10^6$	
Total energy to be stored in capacitors	$W \cdot L/\Delta z$	5×10^8	J

a number of critical open questions could be worked on with relatively little financial effort. They include lifetime studies of repeatedly shock-loaded mm-coils; miniaturization of high-power and high-voltage equipment; technology of filamented, transposed conductors experiencing very high bending strains; ultrahigh vacuum technology in small diameter tubes; economic assessment of low-capacitance, high-voltage capacitors; modelling of the electric circuits in view of inductive coil coupling, coil self-capacitance and lead inductance; and assessment of projectile design in view of heating by ac fields and residual gas. Prior to entering into extensive MAGLAC-studies for impact fusion, a fair comparison with the competing principles of magnetic and inertial confinement should be performed. It must include areas of concern that were not covered in this discussion, e.g., heating of projectile by residual gas, electromagnetic coil coupling, projectile material selection.

8. ACKNOWLEDGEMENT

The author is indepted to his colleagues W. Maurer and J. Erb for valuable discussions.

LIST OF SYMBOLS

A	Cross-section area of projectile
B	Magnetic induction
$B(z)$	Induction along accelerator axis
B_{c2}	Upper critical induction of superconducting projectile
B_{max}	Induction where superconductor has maximum F_v
B_p	Average magnetic induction of projectile to calculate dipole moment
B_{sat}	Saturation induction of ferromagnetic projectile
B_{sc}	Total magnetic induction at superconducting projectile

B_{self}, B_z	Self-field of superconducting projectile
B_0	Peak induction in accelerator coil
C	Capacitance of storage capacitor
E	Dissipated energy in accelerator coils
F_v	Volume pinning force of superconductor
F_{vmax}	Maximum of $F_v(B)$-curve
F_z	Accelerating force along conductor axis
I	Current in accelerator coil
I_0	Amplitude of I
L	Self-inductance of an accelerator coil
N	Number of accelerator coils activated at any instant
P	Joule loss power
R_0	Mean radius of accelerator coil
T	Oscillation period of accelerator coil
T_p	Kinetic energy of projectile
U	Voltage of storage capacitor
V	Volume of projectile
a	Rate of acceleration
b	Magnetic induction normalized to B_{c2}
c_p	Specific heat of accelerator coil material
d	Skin depth
g	Gap between projectile and peak-field region
j	Current density in superconducting projectile
j_c	Critical current density of superconductor
j_0	Amplitude of current density in accelerator coil
l	Length of projectile
m	Mass of projectile
p	Magnetic pressure
r	Radial coordinate of projectile
r_1	Inner radius of magnetically active projectile part
r_2	Outer radius of projectile
t	Thickness of accelerator coil; Time
v	Instantaneous velocity of projectile
v_f	Final velocity of projectile
v_0	Initial velocity of projectile
z	Coordinate along accelerator axis
Δz	Axial length of accelerator coil
$\Delta\theta$	Temperature rise
ϕ	Magnetic flux
α, γ	Parameters
δ	Density of projectile material
μ	Magnetic dipole moment
μ_0	Permeability of vacuum $[= 4\pi \times 10^{-7}(v_s/Am)]$
ν	Oscillation frequency of accelerator circuit
ρ	Resistivity of accelerator coil material
σ	Mechanical stress in magnet coils
τ	Time of energy delivery to pellet

REFERENCES

1. R. L. Garwin, R. A. Muller, B. Richter, JASON-Technical Report ISN-77-20, Dec. 1978 (unpublished).
2. K. W. Chen, IEEE Trans. Nucl. Sci. *NS-26*, 3118 (1979).
3. F. Winterberg, INR Seminar Talk, Kernforschungszentrum Karlsruhe, Sept. 24, 1979 (unpublished); F. Winterberg, Atom Kernenergie *33*, 302 (1979).
4. E. J. Kramer, J. Appl. Phys. *44*, 1360 (1973).